




# Significant enhancement of superconducting performances of Bi-2212 fibers through combined sodium substitution and LFZ process

M. Gürsul<sup>1,\*</sup> , I. Ergin<sup>1</sup>, C. Özçelik<sup>2</sup>, T. Depci<sup>2</sup>, B. Özçelik<sup>1</sup>, M. A. Madre<sup>3</sup>, and A. Sotelo<sup>3</sup>

<sup>1</sup>Department of Physics, Faculty of Sciences and Letters, Çukurova University, 01330 Adana, Turkey

<sup>2</sup>Institute of Engineering and Sciences, Iskenderun Technical University, 31200 Hatay, Turkey

<sup>3</sup>ICMA (CSIC-Universidad de Zaragoza), María de Luna, 50018 Zaragoza, Spain

Received: 26 March 2021

Accepted: 29 May 2021

Published online:

9 June 2021

© The Author(s), under exclusive licence to Springer Science+Business Media, LLC, part of Springer Nature 2021

## ABSTRACT

This paper reports the microstructure, magnetoresistivity, electrical and superconducting properties of Bi-2212 fibers with Na<sup>+</sup> ions incorporated into a superconducting matrix prepared by a polymer solution method and additionally textured through the laser floating zone process. XRD patterns showed that Bi-2212 phase is the major one with mostly (00 $l$ ) diffractions due to the grain alignment, independently of Na content. SEM micrographs showed that samples are composed of well-stacked and oriented grains. The irreversibility field ( $H_{irr}$ ), upper critical magnetic field ( $H_{c2}$ ), coherence length ( $\xi$ ), and activation energies ( $U$ ) have been calculated using magnetoresistivity measurements and explained based on the thermally activated flux flow (TAFF) model. Considering the resistivity-temperature graph for zero field,  $T_c$  values tend to increase from 84.8 K (for the pure sample) to 93.2 K (for 0.075Na sample), slightly decreasing for higher content. Besides, transition temperature width ( $\Delta T_c = T_c^{onset} - T_c^{offset}$ ) decreases with the increment in the Na content and reaches its minimum value ( $\Delta T_c = 3.7$  K) in 0.075Na sample. However, broadening of superconducting transition has been observed with applied field and  $T_c$  values decreased to 76.1 K for the pure sample and 86.8 K for 0.075Na sample. Likewise, the activation energies of the samples also decreases significantly with the increase of the magnetic field and the activation energies of the Na-containing samples are found to be higher than the pure sample at each magnetic field value.  $H_{c2}(0)$  values are calculated as 33.8, 43.8, 50.1, 33.1, and 21.4 T for 0.0, 0.075, 0.10, and 0.20 T Na samples, respectively. As a consequence, referring to all experimental results and theoretical findings, the superconducting characteristics improve regularly with Na-doping until  $x = 0.075$  due to increment in the interaction of superconducting clusters, decrement in weak-links and stabilization of charge carriers in CuO<sub>2</sub> conducting planes.

Address correspondence to E-mail: mgursul@cu.edu.tr

## 1 Introduction

The BSCCO family with  $\text{Bi}_2\text{Sr}_2\text{Ca}_{n-1}\text{Cu}_n\text{O}_{2n+4+y}$  general formula, where  $n = 1, 2,$  and  $3,$  indicating the number of  $\text{CuO}_2$  layers in the unit cell, have three main different phases labeled as Bi-2201, Bi-2212 and, Bi-2223 phases with critical temperatures of about 20, 85, and 110 K, respectively [1, 2]. Among these superconducting phases, the Bi-2212 is stable over a wider temperature range, when compared to the Bi-2223 phase. To obtain promising BSCCO superconducting materials for technological applications intensive studies have been performed. The main goal in most of these studies is to improve the main superconducting parameters such as critical temperature ( $T_c$ ), critical current density ( $J_c$ ), and critical magnetic field ( $H_c$ ) by the addition, doping or substitution process [3–8]. As it is known, the high values of critical temperature and magnetic field are some of the advantages of BSCCO superconductors. On the other hand, the weak-links, high-layered anisotropic structure, disorientation of small grains, and small coherence length are their disadvantages, limiting their technological applications. For many years, researchers have taken into account many applicable strategies to overcome those drawbacks and improving transport properties at 77 K. One of these strategies is based on the BSCCO grain alignment, which allows significantly improving transport properties, compared to the bulk sintered materials. There are several texturing techniques to produce this oriented microstructure in Bi-2212 superconductors, as the hot uniaxial pressing [9], the micropulling down [10], the Laser Floating Zone (LFZ) [11, 12], and the Electrically Assisted Laser Floating Zone (EALFZ) [13]. The grain growth in this system is mainly produced along the ab-plane and, when LFZ technique is used, c-axis is perpendicular to the growth direction provided by the large thermal gradient in the solidification interface. This grain configuration results in maximizing transport properties along the growth axis [14, 15]. When looking at the resistivity-temperature curves, one of the main transport properties of the high- $T_c$  ( $HT_c$ ) granular superconductors like BSCCO, a two-step resistive transition is generally observed. The first step is found in the region where abnormal resistance decreases begins, called onset temperature, while the other one is in the tail region, and called offset temperature. The onset temperature refers to the

occurrence of the superconducting transition of an isolated grain, while the offset temperature at the tail corresponds to intergranular couplings. However, the values of these transition temperatures, especially offset one, significantly drops due to the well-known Lorentz force causing flux-lines motion in the presence of an applied field. In general, the flux-lines motion can be divided into three regions depending on the magnitude of the current applied to the material. These regions are known as flux flow for  $J > J_c$ , thermally activated flux flow (TAFF) for  $J \ll J_c$ , and flux creep between them, where  $J \sim J_c$  [16]. The mechanism that allows overcoming the Lorentz force in a material is called pinning force, which is created by pinning centers. In general, efficient pinning centers can trap the flux-lines and can be naturally formed along grain boundaries, defects, and imperfections, or artificially by chemical substitutions, neutron irradiation, and heavy ion irradiation [17]. Among these methods, chemical substitution is a frequently used method for its usefulness and convenience. Consequently, many different cationic substitutions have been performed to improve superconducting properties of Bi-2212 [18–22].  $\text{Na}^+$  substitution for  $\text{Ca}^{2+}$  that is used in our previous study [22] has yielded quite good results consequently; we have used this substitution in materials textured through LFZ, or hot-forging, for an in-deep investigation of its effect on the physical and superconducting properties of Bi-2212 [23, 24].

In this study, we aim to explore magnetoresistivity, irreversibility and flux pinning energy properties of the  $\text{Bi}_2\text{Sr}_2\text{Ca}_{1-x}\text{Na}_x\text{Cu}_2\text{O}_y$  with  $x = 0.0, 0.05, 0.075, 0.10,$  and  $0.20$  superconducting ceramic rods fabricated via polymer solution method, followed by texturing through the LFZ method. The experimental results will be explained in the framework of the TAFF model using the magnetoresistivity curves obtained at different magnetic fields between 0 and 5 T.

## 2 Experimental procedure

$\text{Bi}_2\text{Sr}_2\text{Ca}_{1-x}\text{Na}_x\text{Cu}_2\text{O}_x$  powders with  $x = 0.0, 0.05, 0.075, 0.10,$  and  $0.20$  were fabricated from commercial metallic acetates ( $\text{CH}_3\text{COO}$ ): Bi ( $\geq 99.99\%$ , Aldrich), Sr (99%, Panreac), Ca (98%, Alfa Aesar), Na ( $\geq 99.99\%$ , Aldrich), and Cu (98%, Panreac). They were processed through a polymer solution

technique described elsewhere [22–24]. The resulting powders obtained were then isostatically pressed in form of cylinders between 2 and 3 mm diameters applying 200 MPa. These cylinders were used as feed in a directional solidification process carried out in an LFZ system with a continuous power Nd:YAG laser with  $\lambda = 1064$  nm. Using a growth rate of 30 mm/h and 18 rpm relative rotation between seed and feed [11], very homogeneous geometrically textured bars of around 2 mm diameter and 120 mm length, were obtained. Due to the incongruent melting of these compounds [25], after the directional solidification process, a thermal treatment was performed to form the Bi-2212 superconducting phase from the Bi-2201, CaCuO<sub>2</sub>, or (Sr,Ca)CuO<sub>2</sub> secondary phases [26]. This thermal process, consisting of two steps (60 h at 860 °C, followed by 12 h at 800 °C), was performed under air. Finally, samples were air-quenched to room temperature. Schematic diagram of the experimental procedure is given in Fig. 1. X-ray powder diffractometer (Rigaku D/max-B, CuK $\alpha$  radiation), with  $2\theta$  ranging between 5 and 60°, was used to obtain the patterns of textured samples. Variation of microstructure of samples, as a function of Na<sup>+</sup> doping level, has been investigated using a field emission scanning electron microscope (FESEM, Zeiss Merlin), together with energy-dispersive X-ray spectroscopy (EDX). Magnetoresistivity measurements were performed under different magnetic fields ranging from 0 to 5 T, employing a conventional four-probe method using a Quantum Design PPMS system following the zero field cooling (ZFC) procedure.

### 3 Results and discussion

X-ray patterns of all fibers have been obtained at room temperature, and presented in Fig. 2a. At first glance, it can be seen that quite similar patterns are obtained for all samples, independently of Na content. The three most intense peaks are recorded at  $2\theta \approx 23.07$ , 29.02 and 35.03° and correspond to the (008), (0010) and (0012) diffraction planes, respectively. In addition to these reflections, relatively low-intensity reflections that are not associated to the *ab*-plane, have also been observed and are marked with “+”. These peaks can be indexed using a pseudotetragonal structure with calculated parameters of  $a-b \approx 5.4$  Å and  $c \approx 30.8$  Å, which are displayed in Table 1 for all

samples. All these results are inconsistent with the lattice parameters of the Bi-2212 phase [27]. On the other hand, to give an idea, XRD results for pure and 0.075 Na fibers, and bulk sintered samples, produced in our previous study [22] are given together in Fig. 2b. From the figure, it can be seen that while reflections in the fiber samples are mostly from the *ab*-plane, in bulk sintered samples a higher number of peaks are observed. The difference between both types of samples can be associated to the different grain sizes obtained in their respective preparation process, much larger in the LFZ one. To evaluate these differences more quantitatively, Lotgering factor (LF) of samples [28], has been calculated. LF is defined as  $(P - P_0)/(1 - P_0)$ , where  $P$  is the sum of the (00 *l*) peak intensities, and  $P_0$  is the sum of the intensities of all peaks of a sample with randomly oriented grains. The obtained results have been 0.48, 0.77, 0.32, and 0.40 for 0, and 0075Na fibers, and 0, and 0.075Na bulk sintered materials, respectively. When evaluating these calculations, it can be concluded that LFZ process drastically raises grain orientation in the samples due to the larger Bi-2212 grains. Moreover, Na<sup>+</sup> substitution further increases these grain sizes, leading to higher grain orientation [22].

The morphological, compositional and microstructural features of samples are investigated by FESEM on longitudinal polished sections presented in Fig. 3. As it can be seen from the pictures, all samples present three different contrasts, associated to three different phases through EDX, identified by arrows and numbers. #1 (white contrast) corresponds to the Bi-2201 phase ( $n = 1$  phase), appearing as minor one, and its content is decreasing up to 0.075Na, slightly increasing for further substitution. #2 (gray contrast) has been identified as Bi-2212 phase ( $n = 2$  phase), as the major one in all cases. Finally, #3 (black contrast) corresponds to the secondary Sr-rich phase found in minor contents which seems to be more or less constant up to 0.10Na substitution, increasing for higher Na content. On the other hand, all samples possess a dense and compact microstructure, with low amount of porosity (an example of porosity has been identified in Fig. 3c. with an arrow), and well-oriented grains, which are typical microstructures of LFZ processed samples [29]. From all these observations, it can be deduced that LFZ processed samples, with the adequate Na substitution, is a very useful technique to produce

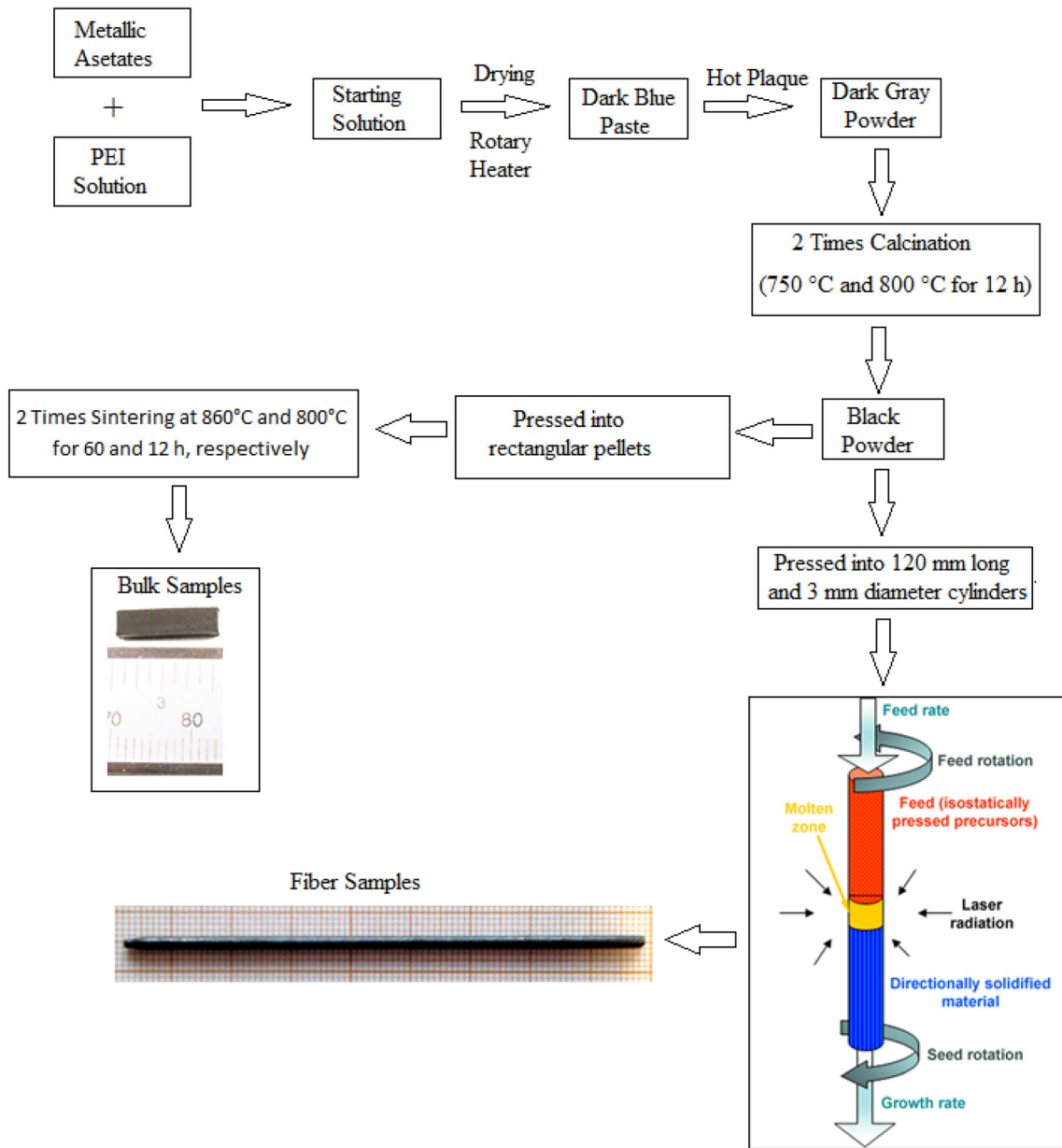


**Fig. 1** Schematic diagram of the experimental procedure

highly oriented grains and high amount of Bi-2212 phase.

The electrical resistivity versus temperature curves for the pristine, and Na-substituted Bi-2212 fibers between 160 and 20 K, are given in Fig. 4a. The inset shows the resistivity plots of pure and 0.075 Na concentrations of bulk and fiber samples for comparison purposes of the effect of LFZ process. Three regimes stand out from these curves for all samples; while the first one is a normal state regime above  $T_c^{onset}$  with a linear behavior, the second is the zone between  $T_c^{onset}$  and  $T_c^{offset}$  with non-linear type

behavior resulting from the fluctuation of Cooper pair, and the last one is the region below  $T_c^{offset}$  where phase-coherence of Cooper pairs reaches its optimum state as a result of interlayer coupling revealing practically zero resistance in the materials. In the normal state, all samples exhibit metallic behavior ( $d\rho/dt > 0$ , see Fig. 4b), and resistivity curves can be accurately fitted by well-known Matthiessen’s rule given by  $\rho = \rho_0 + aT$  where  $\rho_0$  is temperature-independent residual resistivity resulting from defects such as cracks, voids, stack faults, and dislocations or misorientation of successive  $\text{CuO}_2$

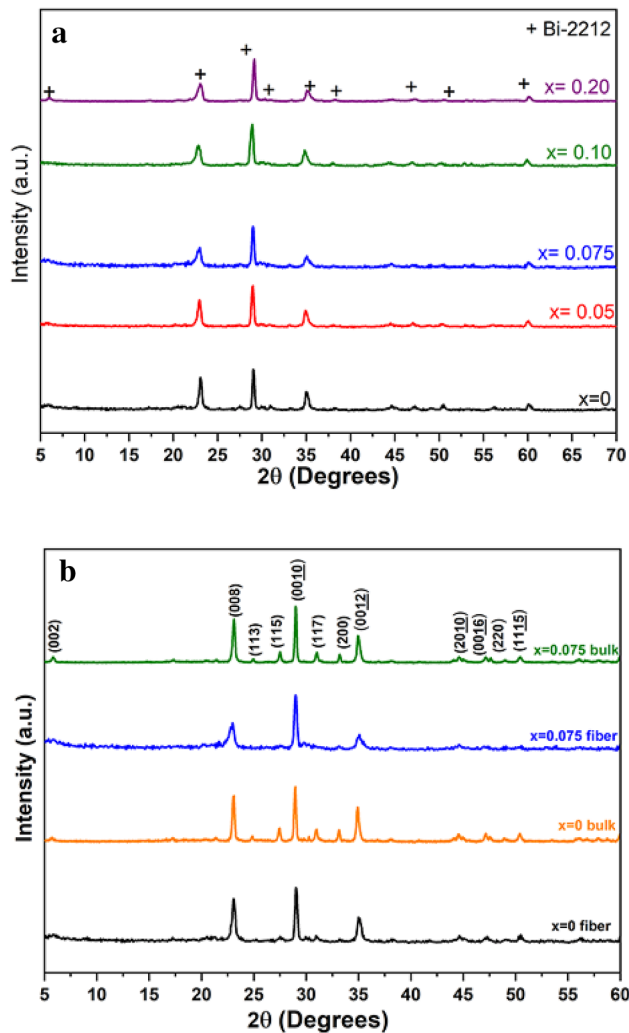


**Fig. 2** XRD patterns of **a** Fiber samples **b** Fiber versus bulk samples

planes in the system [30–33].  $\rho_0$  values determined from the extrapolations of normal state resistivity curves is depicted in the inset of Fig. 4b for Na-free samples and are given in Table 1 for all samples. The

minimum  $\rho_0$  value (0.08 m $\Omega$ .cm) has been obtained in 0.05Na samples, reflecting the effect of grain alignment produced by the LFZ process as shown in Fig. 1, and observed in FESEM micrographs (see Fig. 3). In spite of the very close values obtained in 0.075Na doped samples, this value goes into an increasing trend in samples with higher Na substitution, reaching 1.67 m $\Omega$  cm in 0.20Na samples. This evolution clearly indicates an increment in the permanent defects in the crystal when the Na substitution is > 0.075, probably due to the larger formation of Sr-rich secondary phase. The peak position in the  $d\rho/dt$  versus temperature graph shown in Fig. 4b corresponds to the samples  $T_c$ . According to the figure, two peaks around 118 and 82 K were observed in the bulk sintered Na-free samples, which indicate the presence of Bi-2223, and Bi-2212 phases, respectively. However, in LFZ processed samples, the Bi-2223 phase in the system disappeared and only the peak corresponding to the Bi-2212 is observed. Also, as shown in Fig. 4b the full width at half maximum (FWHM) of the resistive differentiation curve also decrease from 5.2 to 3.3 after the LFZ process. Thus, these results also express the capacity of the LFZ process to form homogenous superconducting clusters. In addition to these advantages, Na substitution also provides additional improvements to the Bi-2212 system, significantly increasing  $T_c$  as shown in Table 1.  $T_c$  values tend to increase from 84.8 K (for the pure samples) to 93.2 K (for 0.075Na samples), slightly decreasing for higher content, even if for 0.20Na samples the  $T_c$  value (90.8 K) is still much higher than the measured in the pure ones. In addition to this improvement, transition temperature width ( $\Delta T_c = T_c^{\text{onset}} - T_c^{\text{offset}}$ ), given in Table 1, tends to decrease with the increment in the Na content and reaches its minimum value ( $\Delta T_c = 3.7$  K) in 0.075Na

**Table 1** Structural and transport properties of all samples

Sample	Unit-cell parameter (Å)		$\rho_0$ (m $\Omega$ cm)	$T_c$ (K)	$\Delta T_c$ (K)	$p$	$S$ ( $\mu$ V/K)
	$a \approx b$	$c$					
$x = 0$	5.445	30.732	0.14 (Bulk: 1.56)	84.8 (Bulk: 82.5)	6.5	0.197	1.63
$x = 0.05$	5.451	30.806	0.08	92.6	4.1	0.180	11.21
$x = 0.075$	5.448	30.761	0.09 (Bulk: 0.41)	93.2 (Bulk: 83.1)	3.7	0.178	12.38
$x = 0.10$	5.459	30.874	0.34	91.8	3.8	0.182	10.04
$x = 0.20$	5.446	30.695	1.67	90.8	3.9	0.185	8.32

**Fig. 3** FESEM micrographs of the samples

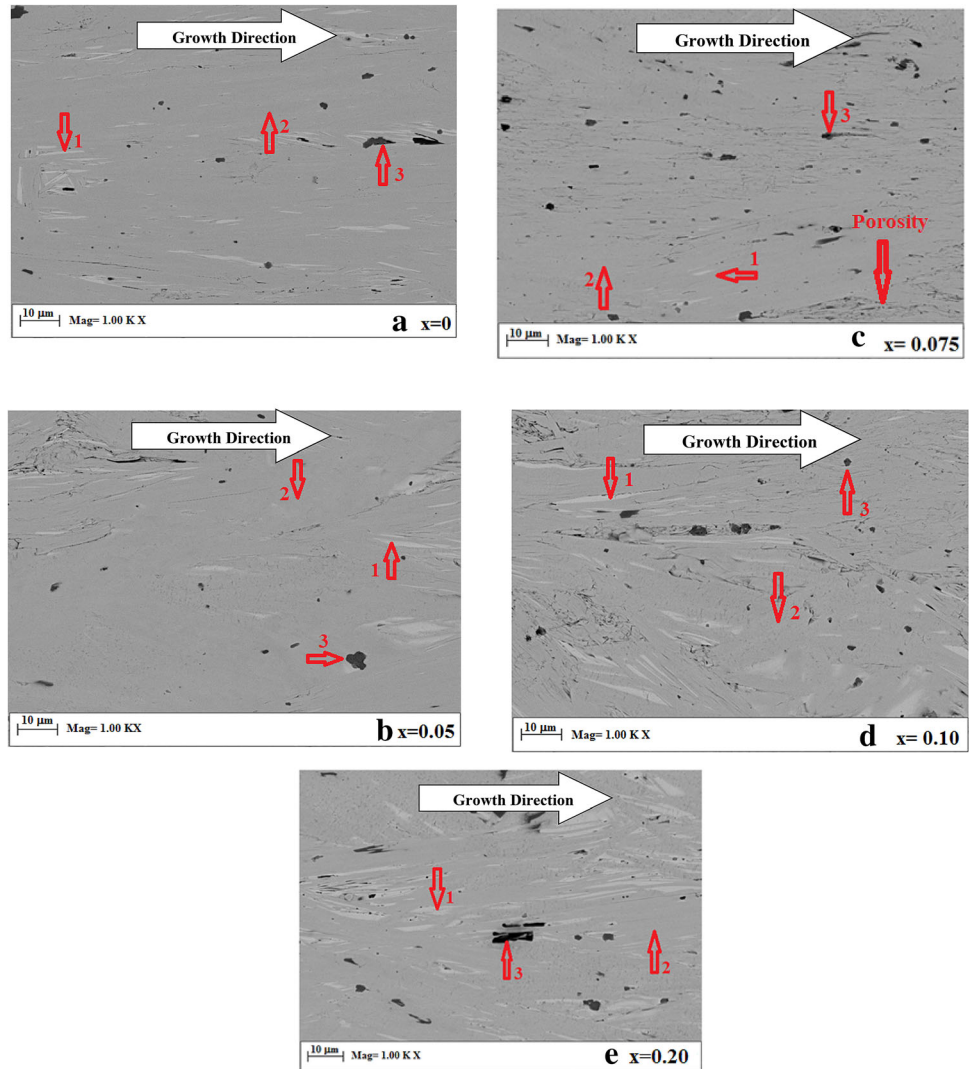
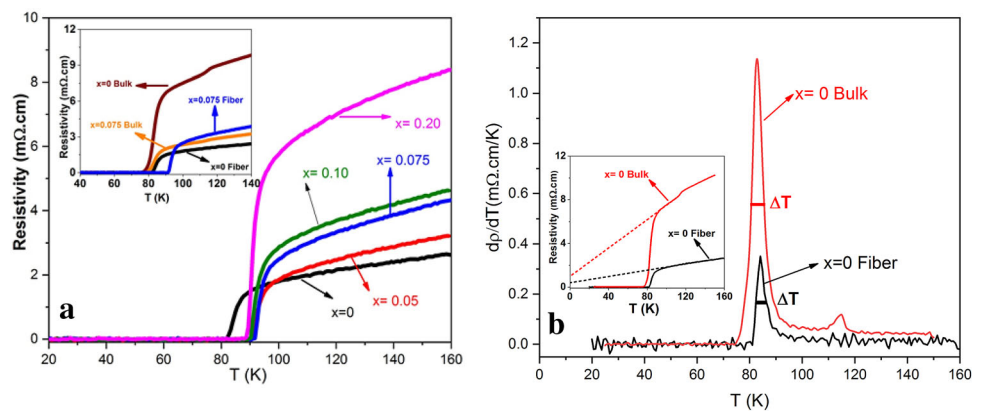


**Fig. 4** **a** DC electrical resistivity versus temperature curves for all samples. **b**  $d\rho/dT$  versus temperature curves of all samples



samples. It seems that replacing  $\text{Ca}^{2+}$  with  $\text{Na}^{+}$  with lower valence, but similar ionic radii, stabilizes superconducting clusters and optimizes mobile hole carrier concentration in  $\text{CuO}_2$  planes of Bi-2212

phase. In fact, due to the similar ionic radii of  $\text{Ca}^{2+}$  and  $\text{Na}^{+}$ , introduction of Na into the Bi-2212 structure is an effective hope-doping process inducing extra charge carriers into the  $\text{CuO}_2$  planes. X-ray

absorption fine structure (XAFS) studies showed that by Na-doping, Cu valence increases from + 2.109 to + 2.194 and more carriers can be transferred to the CuO<sub>2</sub> planes, leading to enhanced  $T_c$  [34]. To calculate mobile hole concentrations ( $p$ ) per CuO<sub>2</sub> plane, an empirical formula proposed by Presland et al. [35] can be used:

$$T_c/T_c^{\max} = 1 - 82.6(p - 0.16)^2 \quad (1)$$

where  $T_c^{\max}$  is taken as 95 K for the Bi-2212 superconducting system and  $T_c$  corresponds to the peak positions of  $d\rho/dt$  versus temperature graph of zero field resistivity experiments tabulated in Table 1. According to the numerical results given in Table 1, the values range from 0.178 to 0.197 and are far from the over-doped or under-doped limits.

Using hole concentration values displayed in Table 1, thermoelectric power,  $S$ , of the samples can be calculated using the following equation [36]:

$$S = \frac{k_B}{|e|} \left[ \ln \frac{1-p}{2p} - \ln 2 \right] \quad (2)$$

where  $p$ ,  $k_B$  and  $e$  are the hole concentration, Boltzmann constant, and electron charge, respectively. Considering the calculation results embedded in Table 1, all  $S$  values are positive which is an indication of hole-dominated transport mechanisms in the samples, reaching the highest value (12.38  $\mu\text{V}/\text{K}$ ) in 0.075Na samples.

The magnetoresistivity experiments in the temperature range of 20–160 K were carried out at three different magnetic field values, 1, 3, and 5 T, and the results are shown in Fig. 5. From these curves, transition temperatures  $T_c^{\text{onset}}$ , related to the transition of isolated grains, and  $T_c^{\text{offset}}$ , attributed to interlayer coupling and the volume fraction of the Bi-2212 phase, have been obtained and tabulated in Table 2. At first sight, it seems that, while the  $T_c^{\text{onset}}$  values of samples are almost the same,  $T_c^{\text{offset}}$  ones dramatically decrease. With the increase of superconducting charge carriers in the intergranular regions, there is no flux trapping in these regions and thus  $T_c^{\text{onset}}$  values are not severely affected by the magnetic field. On the other hand, the broadening effect observed at the tail part of the resistivity curves, and  $T_c^{\text{offset}}$  values have been drastically lowered by increasing the magnetic field. These significant decreases in  $T_c^{\text{offset}}$  values can be attributed to a reduction of pinning ability as a result of increasing weak-links between superconducting grains at higher magnetic fields.

With increasing magnetic field,  $T_c^{\text{offset}}$  values decreased from 82.7 to 55.4 K for 0Na, from 91.3 to 66.1 K for 0.05Na, from 92.0 to 69.1 K for 0.075Na, from 90.5 to 63.2 for 0.10Na, and from 89.5 to 54.1 K for 0.20Na samples. From these numerical values, it is clear that  $T_c^{\text{offset}}$  values of all Na-containing samples are higher than the determined in the pure ones. It may be concluded that Na<sup>+</sup> causes the raise of the carrier concentrations in CuO<sub>2</sub> conduction planes, together with the increase of superconducting volume fraction, as previously discussed in XRD and FESEM-EDX analysis. Further, an obvious rise in  $T_c^{\text{offset}}$  values can be attributed to stronger intragrain pinning energy in Na-containing samples performing a higher resistance to the vortex motion in the vicinity of  $T_c$  [37].

As it is well known, if the pinning force in the matrix is adequately strong, vortex motion is restricted and the superconductor behaves similarly to a perfect conductor. If a strong current is applied to superconducting materials, due to dissipative Lorentz force, the thermally activated flux creep can always be observed and the vortices can hop from one pinning site to another at an observable rate [38]. Using the experimental findings of magnetoresistivity curves obtained under of 0, 1, 3 and 5 T magnetic fields, the Thermally Activated Flux Flow (TAFF) model has been used to investigate the variation of activation energy, irreversibility field, upper critical field, and coherence length of the samples, caused by Na substitution. According to TAFF model, the dissipation energy in the tail part of the magnetoresistance curve is explained by an Arrhenius-type equation given in [38, 39]

$$\rho(H, T) = \rho_0 \exp(-U(H)/k_B T) \quad (3)$$

where  $U$  is known as the flux pinning or activation energy depending on temperature and magnetic field,  $\rho_0$  is the pre-exponential factor, and  $k_B$  is Boltzmann constant. The tail part of the resistivity curve is tremendously vulnerable to the magnetic field and the expanding in the curve is inversely proportional to the magnitude of flux pinning energy. To have a numerical indication about the activation energies magnitudes, the natural logarithm in both sides of magnetoresistance expression is taken, and  $\ln(\rho/\rho_0)$  versus  $1/T$  graphs of the samples are presented in Fig. 6. From the figure, a very clear shift toward lower temperatures with the increment of the magnetic field can be observed. This shifting

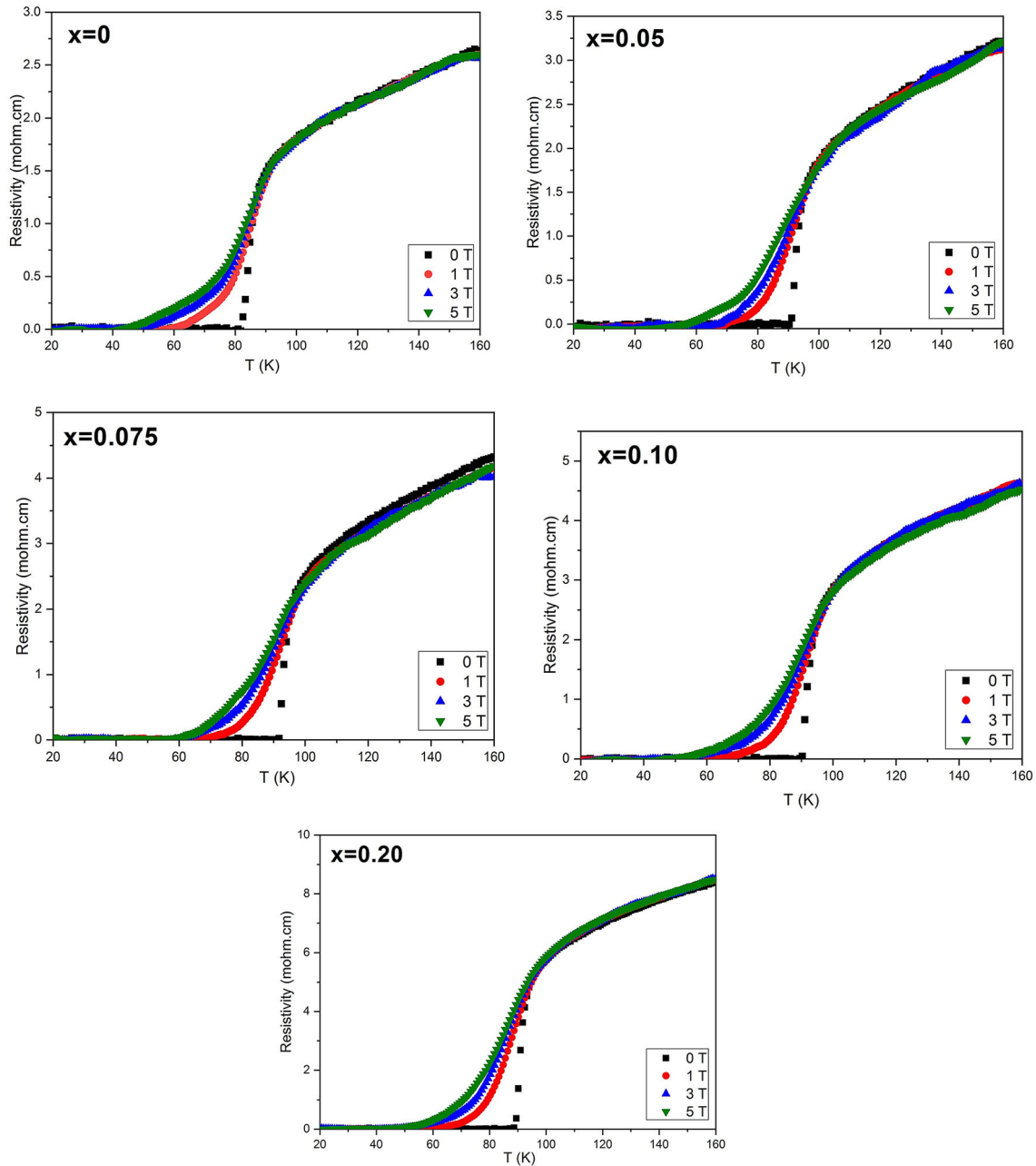


**Fig. 5** Magnetoresistivity curves for all samples

behavior is related to the flux flow resistivity referred to the fact that reducing temperature, the pinning force is enhanced. Furthermore, an exponential behavior of  $\rho$  to  $1/T$  for temperature below  $T_c^{\text{onset}}$  is observed, which can be an indication of the energy dissipation in the thermally activated flux flow region owing to the fluxons hopping across the pinning barriers as a result of thermal energy. Hence, the flux pinning energy,  $U$ , value is directly deduced from the slope of the straight-line portions of the graphs. The

flux pinning or activation energy,  $U$ , concerning the external applied magnetic field is presented in Fig. 7, for all samples.  $U$  values are drastically decreased by increasing the applied magnetic field and significantly increased with the increment of Na amount. In this step, it can be argued that the increment of the energy barriers, are due to an increase in the number of pinning centers, which decreases the magnetic field penetration in the samples. At this stage, an increase of the intergranular coupling arises, and the



**Table 2** Some physical findings using magnetoresistivity curves for all samples

Sample	Temp	0 T	1 T	3 T	5 T	$\beta$	$n$	$q$	$H_{irr}(0\text{ K})(T)$	$H_{c2}(0\text{ K})(T)$	$\xi$ (Å)
$x = 0$	$T_c^{\text{onset}}$	89.2	88.3	87.2	86.1	0.45	0.30	1.50	23.7	33.8	31.2
	$T_c$	84.8	81.9	78.6	76.1						
	$T_c^{\text{offset}}$	82.7	69.4	61.3	55.4						
$x = 0.05$	$T_c^{\text{onset}}$	95.4	94.9	93.5	92.1	0.47	0.23	2.04	30.4	43.8	27.4
	$T_c$	92.6	90.2	87.5	85.2						
	$T_c^{\text{offset}}$	91.3	77.1	71.3	66.1						
$x = 0.075$	$T_c^{\text{onset}}$	95.7	95.4	93.9	92.4	0.40	0.24	1.66	32.1	50.1	25.6
	$T_c$	93.2	90.6	88.4	86.8						
	$T_c^{\text{offset}}$	92.0	79.3	74.2	69.1						
$x = 0.10$	$T_c^{\text{onset}}$	94.3	92.8	91.0	89.6	0.36	0.26	1.38	30.8	33.1	31.5
	$T_c$	91.8	88.9	85.4	82.0						
	$T_c^{\text{offset}}$	90.5	75.7	68.1	63.2						
$x = 0.20$	$T_c^{\text{onset}}$	93.4	89.5	85.8	84.2	0.38	0.33	1.15	18.5	21.4	39.2
	$T_c$	90.8	84.2	79.6	76.4						
	$T_c^{\text{offset}}$	89.5	72.2	62.1	54.1						

vortices cannot easily creep due to the higher activation energy. Besides, it is necessary to mention that the external magnetic field can diffuse the intergranular region depending on the proportions of weak-links or couplings of the superconducting grains and clusters in the material of interest. Therefore, the strong-links between clusters in 0.075Na samples are larger than those of the other ones.

The flux pinning energy can be described by a power-law as

$$U(H) \approx H^{-\beta} \quad (4)$$

where  $\beta$  corresponds to the orientation of the applied field in terms of the basal plane [40]. The  $\beta$  values have been calculated and tabulated in Table 2 using the deduced values for pinning energy,  $U$ , plotted in Fig. 7. According to the table, the  $\beta$  values are lower Mn-substituted BiPb-2223 samples [41], but higher than the obtained in BaSnO<sub>3</sub> added BiPb-2223 system ( $\beta \approx 0.22$ – $0.25$ ) [40]. We should emphasize here that  $\beta$  depends on many parameters influencing the pinning energy and the properties of crystal structure, as the quality of weak-links, real atomic positions and oxygen content [40]; therefore, there are no predictable values for it.

The magnetic field dependence of the transition temperature width  $\Delta T$  ( $= T_c^{\text{onset}} - T_c^{\text{offset}}$ ) is determined using a power-law relation as [40]

$$\Delta T \approx H^n \approx H^{\beta/q} \quad (5)$$

The magnetic field dependence of  $\Delta T$  is exhibited in Fig. 8 for all samples. As it can be easily observed, when the applied magnetic field increase,  $\Delta T$  values monotonically increase. The reason for these increments in  $\Delta T$  with increasing the magnetic field,  $H$ , can be associated to the freezing of several grains and clusters in random positions during cooling, causing more resistive domains in the matrix. Thus, these regions lead to the damping of vortex pinning strength as a consequence of the reduction of the superconducting current path [40]. Besides, the reduction in  $\Delta T$  with an increment of the Na substitution may be attributed to a reduction of microscopic nonuniform superconducting phases and/or an increase of intergrain coupling. Using these experimental results, and by plotting  $\Delta T$  versus applied magnetic field in log–log scale  $n$  and  $q$  parameters were obtained and tabulated in Table 2. The fact that  $n$  values are lower in Na-substituted samples than in undoped ones, except for 0.20Na ones, can be seen as evidence showing that samples containing Na

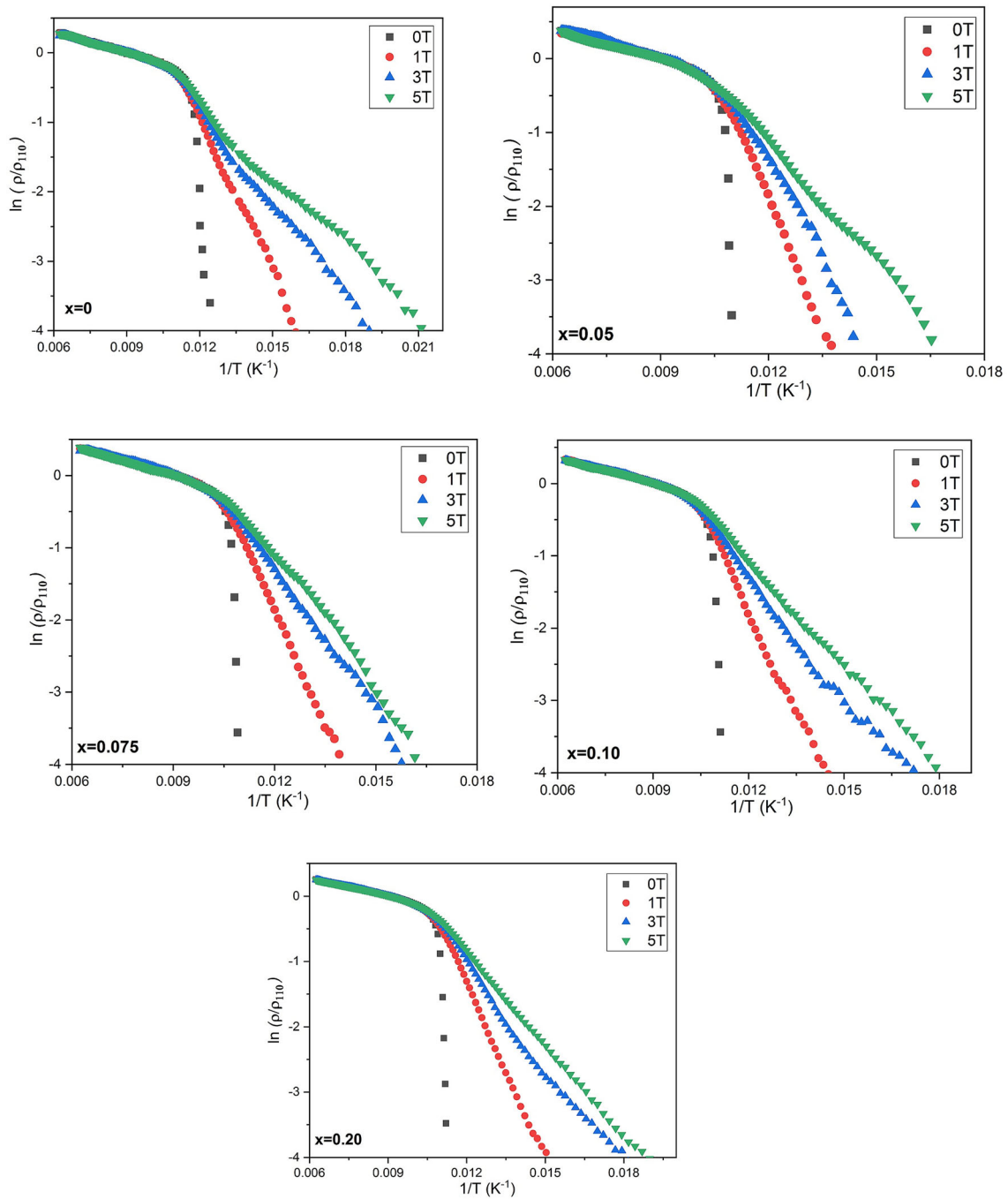


**Fig. 6**  $\ln(\rho/\rho_{110})-1/T$  plot of the samples

up to a certain amount have higher superconducting properties.

The irreversibility field line (IL) in high- $T_c$  type II superconductors corresponds to the transition from the region where flux pinning is dominant to the TAFF region, where the resistance resulting from flux flow occurs. IL separates the  $H-T$  plane into two different regimes. These regimes are designated high-

temperature regime where the fluxes freely move and magnetically reversible and low-temperature regime, in which the flux dynamics are dissipative and consequently irreversible. To deduce IL, a plot of irreversibility magnetic field,  $H_{irr}$ , values with respect to offset temperatures,  $T_c^{offset}$  is shown in Fig. 9 for all the samples. It is clear from the graph that as the temperature decreases, the  $H_{irr}$  increases toward high

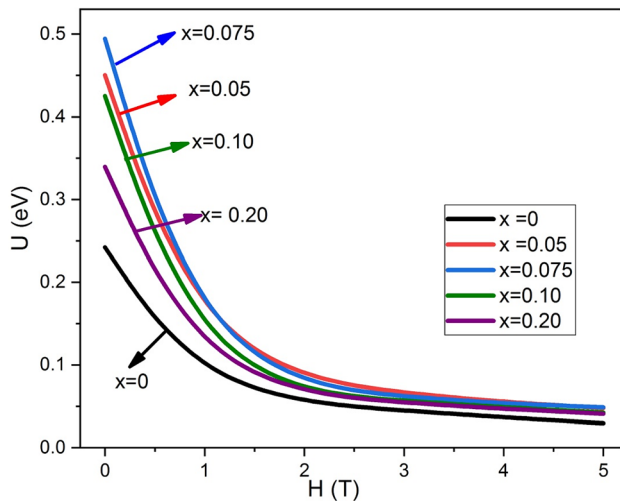


**Fig. 7** Activation energies of all samples

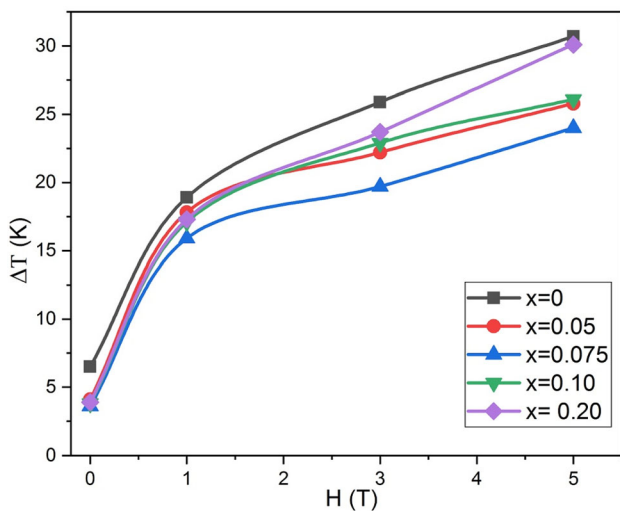


**Fig. 8**  $\Delta T$  versus  $H$  curves for the samples

fields values for all samples. In addition, when compared with the pure sample, the position of the IL of Na-substituted samples (except for 0.20Na ones) shifts toward high-temperature values. This behavior points out to the strength reinforcement of vortex fluctuations by increasing Na content.

The upper critical field,  $H_{c2}(T)$ , is an important parameter for the technological applications of superconductors. For a given temperature, it describes the maximum magnetic field strength below which the superconducting properties of materials are preserved. The plot of  $H_{c2}(T)$  against the critical temperature, 50%  $T_c$  midpoint, is shown in Fig. 10. From the figure, it seems that the curves of 0.05, 0.075, and 0.10Na are shifted toward higher

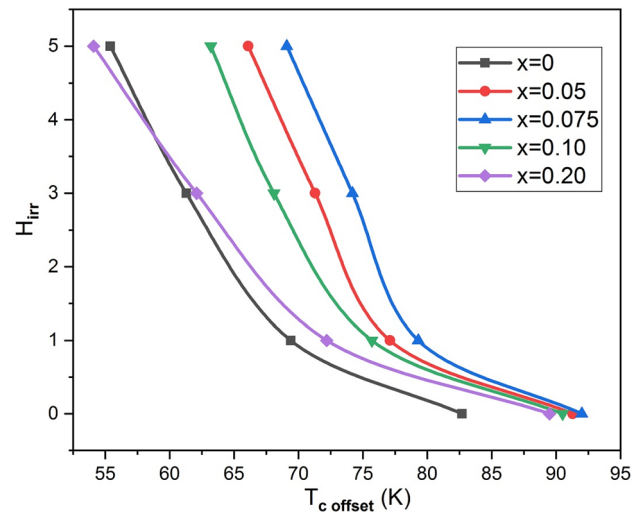


**Fig. 9**  $H_{irr}$ - $T_c^{\text{offset}}$  curves for the samples

temperatures than that of the pure samples. This is another evidence of higher activation energy of the pinning centers in Na-containing samples. On the other hand, the shift in 0.20Na samples is very sensitive to the magnetic field, and its curve coincides with the curve of the pure ones at 5 T. Even more interestingly, from the trend of these curves, it can be predicted that the shift will be toward the lowest temperature values among all samples. Thus, this content can be considered excessive, as it lowers the melting point in the system, thereby reducing the strength of energy barriers in the pinning centers, and resulting in lower activation energies at higher magnetic fields. In a related manner, to identify  $H_{c2}(T)$  variation against temperature, an empirical

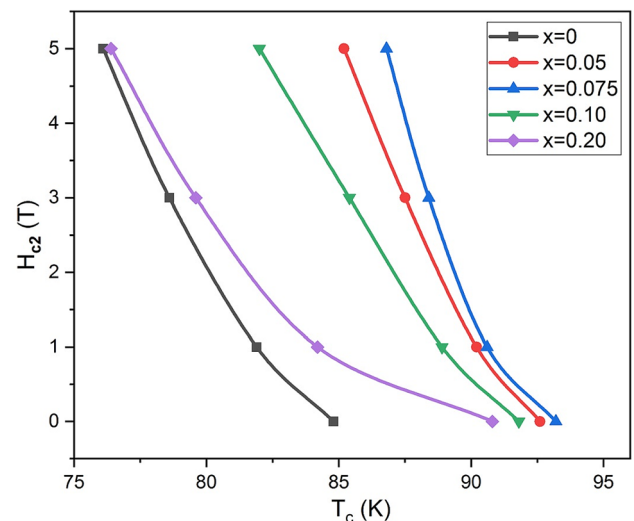


**Fig. 10**  $H_{c2}$  versus  $T_c$  curves of the samples

formula suggested by Werthamer–Helfand–Hohenberg (WHH) [42, 43] as

$$H_{c2}(0) = 0.693T_c[dH_{c2}(T)/dT]_{T_c} \quad (6)$$

can be used. Here, the  $[dH_{c2}(T)/dT]$  values are found using  $T_c$  values determined from the peak position in the  $d\rho/dt$  versus temperature graph shown in Fig. 4b. Considering  $H_{c2}$  values embedded in Table 2, calculations were obtained in accordance with the main theme given in the article, that is, it reached the maximum value of 50.1 T in 0.075Na samples, decreasing for higher Na content, and reaching the minimum value in 0.20Na ones.

Finally, the coherence length,  $\xi$ , is another important and characteristic parameter of the superconductors and can be obtained from the Ginzburg–Landau relation [44]:

$$\mu_0 H_{c2}(0) = \Phi_0 / 2\pi\xi^2(0) \quad (7)$$

where  $\Phi_0$ , the quanta of flux, is  $2.07 \times 10^{-15}$  T.m<sup>2</sup> value, and  $H_{c2}(0)$ , the upper critical field at zero temperature, is found above. The obtained  $\xi$  values are tabulated in Table 2. Depending on the  $H_{c2}(0)$ ,  $\xi$  values vary between 25.6 to 39.2 Å, in agreement with the typical values reported in the literature [45, 46].

## 4 Conclusions

Bi<sub>2</sub>Sr<sub>2</sub>Ca<sub>1-x</sub>Na<sub>x</sub>Cu<sub>2</sub>O<sub>8+y</sub> fibers with  $x = 0.0, 0.05, 0.075, 0.10,$  and  $0.20$  has been fabricated using a polymer solution method, followed by texturing through the LFZ technique. The fact that most of the peaks of XRD correspond to (00 l) planes of the Bi-2212 phase indicates the success of the LFZ process in grain orientation. Further, Na<sup>+</sup> doping further enhances the grain orientation, which is confirmed through Lotgering factor. According to SEM–EDS analysis, while the samples possess a dense microstructure with a low amount of porosities and well-oriented grains as a result of LFZ, Na substitution also helps to reduce the amount of secondary phases.  $T_c$  values tend to increase from 84.8 K (for the pure sample) to 93.2 K (for 0.075Na sample), slightly decreasing for higher content. In addition, transition temperature width ( $\Delta T_c$ ) decreases with the increment in the Na content and reaches its minimum value ( $\Delta T_c = 3.7$  K) in 0.075Na sample.  $T_c^{\text{offset}}$  values

decreased dramatically with the increase of the magnetic field, such that in the pure sample  $T_c^{\text{offset}}$  value is 86 K at 0 T, decreases to 55 K at 5 T, and in the 0.075 sample, this decrease is relatively less, and at 0 T, it is 92 K and falls to 69.1 K at 5 T. The improvement of the calculated flux pinning energy, irreversibility field, and upper critical field with increasing Na content up to 0.075 has been observed. Hence, it can be concluded that this content is the optimum one leading to effective pinning centers, reinforcing intergranular coupling.

## Acknowledgements

A. Sotelo and M. A. Madre acknowledge Spanish MINECO-FEDER (Project MAT2017-82183-C3-1-R) and Gobierno de Aragón-FEDER (Research Group T 54-20R) for funding. Authors would like to acknowledge the use of Servicio General de Apoyo a la Investigación-SAI, Universidad de Zaragoza.

## References

1. H. Maeda, Y. Tanaka, M. Fukutomi, T. Asano, K. Togano, H. Kumakura, M. Uehara, S. Ikeda, K. Ogawa, S. Horiuchi, Y. Matsui, New high-Tc superconductors without rare earth element. *Physica C* **153–155**, 602–607 (1988)
2. C. Michel, M. Hervieu, M.M. Borel, A. Grandin, F. Deslandes, J. Provost, B. Raveau, Superconductivity in the Bi-Sr-Cu-O system. *Zeitschrift für Physik B* **68**, 421–423 (1987)
3. A. Biju, K. Vinod, R.P. Aloysius, U. Syamaprasad, Improved superconducting properties by La addition in (Bi, Pb)-2212 bulk superconductor. *J. Alloys Compd.* **431**, 49–55 (2007)
4. A. Sedky, W. Al-Battat, Effect of Y substitution at Ca site on structural and superconducting properties of Bi:2212 superconductor. *Phys. B* **410**, 227–232 (2013)
5. S. Vinu, P.M. Sarun, A. Biju, R. Shabna, P. Guruswamy, U. Syamaprasad, The effect of substitution of Eu on the critical current density and flux pinning properties of (Bi, Pb)-2212 superconductor. *Supercond. Sci. Technol.* **21**, 045001–045005 (2008)
6. K. Yorimasa, M. Uehara, T. Kuramoto, H. Inoue, Y. Kimishima, S-doping effects on pinning property of Bi2212 single crystals. *Physica C* **392–396**, 306–310 (2003)
7. S. Bal, M. Dogruer, G. Yildirim, A. Varilci, C. Terzioglu, Y. Zalaoglu, Role of cerium addition on structural and superconducting properties of Bi-2212 system. *J. Supercond. Novel Magn.* **25**, 847–856 (2012)

8. B. Özkurt, Enhancement in superconducting transition temperature and  $J_c$  values in Na-doped  $\text{Bi}_2\text{Sr}_2\text{Ca}_1\text{Cu}_{2-x}\text{Na}_x\text{O}_y$  superconductors. *J. Mater. Sci.* **24**, 2426–2431 (2013)
9. X.K. Fu, Y.C. Guo, W.M. Chen, H.K. Liu, S.X. Dou, Effect of the sinter-forging deformation rate on properties of Bi-2223 current leads. *IEEE Trans. Appl. Supercond.* **11**, 2551–2554 (2001)
10. K. Lebbou, A. Yoshikawa, M. Kikuchi, T. Fukuda, M.T. Cohen-Adad, G. Boulon, Superconductor Bi2212 fiber growth from the melt by micro-pulling down technique. *Physica C* **336**, 254–260 (2000)
11. M.F. Carrasco, F.M. Costa, R.F. Silva, F. Gimeno, A. Sotelo, M. Mora, J.C. Díez, L.A. Angurel, Textured Bi–Sr–Ca–Cu–O rods processed by laser floating zone from solid state or melted precursors. *Physica C* **415**, 163–171 (2004)
12. B. Özkurt, M.A. Madre, A. Sotelo, M. Eyyüphan Yakıncı, B. Özçelik, Relationship between growth speed, microstructure, mechanical and electrical properties in Bi-2212/Ag textured composites. *J. Supercond. Nov. Magn.* **25**, 799–804, (2012)
13. M.F. Carrasco, V.S. Amaral, R.F. Silva, F.M. Costa, Electrical assisted laser floating zone (EALFZ) growth of 2212-BSCCO superconducting fibres. *Appl. Surf. Sci.* **257**, 5283–5286 (2011)
14. G.F. de la Fuente, M.T. Ruiz, A. Sotelo, A. Larrea, R. Navarro, Microstructure of laser floating zone (LFZ) textured (Bi, Pb)-Sr-Ca-Cu-O superconductor composites. *Mater. Sci. Eng. A* **173**, 201–204 (1993)
15. F.M. Costa, M.F. Carrasco, R.F. Silva, J.M. Vieira, Trapping control of phase development in zone melting of Bi Sr Ca Cu O superconducting fibres. *Supercond. Sci. Technol.* **16**, 392–397 (2003)
16. D. Sharma, R. Kumar, V.P.S. Awana, Temperature and field dependence of thermally activated flux flow resistance in  $\text{Bi}_2\text{Sr}_2\text{CaCu}_2\text{O}_{8+\delta}$  superconductor. *Solid State Commun.* **152**, 941–946 (2012)
17. J. Trastoy, V. Rouco, C. Ulysse, R. Bernard, G. Faini, J. Lesueur, J. Briatico, J.E. Villegas, Nanostructuring of high-TC superconductors via masked ion irradiation for efficient ordered vortex pinning. *Physica C* **506**, 195–200 (2014)
18. R.P. Aloysius, P. Guruswamy, U. Syamaprasad, Highly enhanced critical current density in Pr-added (Bi, Pb)-2212 superconductor. *Supercond. Sci. Technol.* **18**, L23–L28 (2005)
19. A. Biju, R.P. Aloysius, U. Syamaprasad, *Supercond. Sci. Technol.* **18**, 1454–1459 (2005)
20. Y.P. Sun, W.H. Song, B. Zhao, J.J. Du, H.H. Wen, Z.X. Zhao, H.C. Ku, Improved flux pinning and anomalous magnetization peak in heavily overdoped  $\text{Bi}_{2-x}\text{Pb}_x\text{Sr}_2\text{CaCu}_{2-y}\text{Cr}_y\text{O}_{8+\delta}$  single crystals. *Appl. Phys. Lett.* **76**, 3795 (2000)
21. S. Zhang, M. Liang, C. Li, Q. Hao, J. Feng, P. Zhang, Enhanced flux pinning properties in Bi-2212 high temperature superconductors with nano-sized precipitates. *Mater. Lett.* **157**, 197–200 (2015)
22. B. Özçelik, M. Gürsul, A. Sotelo, M.A. Madre, Improvement of superconducting properties in Na-doped BSCCO superconductor. *J. Mater. Sci.: Mater. Electron.* **26**, 441–447, (2015)
23. O. Nane, B. Özçelik, A. Sotelo, M.A. Madre, Effect of Na substitution on superconducting properties of Bi-2212 ceramics prepared by Sinter-Forged process. *J. Eur. Ceram. Soc.* **37**, 1007–1012 (2017)
24. O. Nane, B. Özçelik, H. Amaveda, A. Sotelo, M.A. Madre, Improvement of structural and superconducting properties of Bi-2212 textured rods by substituting sodium. *Ceram. Int.* **42**, 8473–8477 (2016)
25. M. Mora, A. Sotelo, H. Amaveda, M.A. Madre, J.C. Díez, F. Capel, J.M. López-Cepero, Properties variation of Bi-2212 directionally solidified induced by 0.4Pb substitution. *J. Eur. Ceram. Soc.* **27**, 3959–3962, (2007)
26. F.M. Costa, R.F. Silva, J.M. Vieira, Phase transformation kinetics during thermal annealing of LFZ Bi–Sr–Ca–Cu–O superconducting fibers in the range 800–870°C. *Physica C* **323**, 23–41 (1999)
27. X. Zhao, W. Wu, X. Sun, X.-G. Li, New experimental evidence of the structural modification in single crystal  $\text{Bi}_2\text{Sr}_2\text{CaCu}_2\text{O}_y$  by X-ray diffraction observation. *Physica C* **320**, 225–232 (1999)
28. F.K. Lotgering, Topotactical reactions with ferrimagnetic oxides having hexagonal crystal structures—II. *J. Inorg. Nucl. Chem.* **16**, 100–108 (1960)
29. A. Sotelo, M.A. Madre, J.C. Díez, S. Rasekh, L.A. Angurel, E. Martínez, The influence of Pb and Ag doping on the  $J_c(H, T)$  dependence and the mechanical properties of Bi-2212 textured rods. *Supercond. Sci. Technol.* **22**, 034012, (2009)
30. A.T. Ülgen, T. Turgay, C. Terzioglu, G. Yildirim, M. Oz, Role of Bi/Tm substitution in Bi-2212 system on crystal structure quality, pair wave function and polaronic states. *J. Alloys Compd.* **764**, 755–766 (2018)
31. G. Yildirim, Determination of optimum diffusion annealing temperature for Au surface-layered Bi-2212 ceramics and dependence of transition temperatures on disorders. *J. Alloys Compd.* **699**, 247–255 (2017)
32. N.K. Saritekin, M. Oz, C. Terzioglu, O. Gorur, G. Yildirim, Significant development on pinning of vortices in Y-123 superconductor with homovalent Ba/Nd substitution. *J. Mater. Sci.: Mater. Electron.* **27**, 6992–7003, (2016)
33. R. Kalyanaraman, S. Oktyabrsky, J. Narayan, The role of Ag in the pulsed laser growth of YBCO thin films. *J. Appl. Phys.* **85**, 6636–6641 (1999)

34. J.Y. Oh, D.S. Yang, D.H. Tran, B. Kang, Influences of N-doping on valence states and interatomic potential in  $\text{Bi}_{1.6}\text{Pb}_{0.4}\text{Sr}_2\text{Ca}_2\text{Cu}_3\text{O}_{10+\delta}$  superconductor, *Ceram. Int.* **46**, 8259–8263, (2020)
35. M.R. Presland, J.L. Tallon, R.G. Buckley, R.S. Liu, N.E. Flower, General trends in oxygen stoichiometry effects on  $T_c$  in Bi and Tl superconductors. *Physica C* **176**, 95–105 (1991)
36. M. Chandra Sekhar, S.V. Suryanarayana, Thermoelectric power in  $\text{Bi}_2\text{Sr}_{2-x}\text{K}_x\text{CaCu}_2\text{O}_y$ , *Physica C* **415**, 209–219, (2004)
37. B. Özkurt, B. Özçelik, Effect of Nd-substitution on thermally activated flux creep in the  $\text{Bi}_{1.7}\text{Pb}_{0.3-x}\text{Nd}_x\text{Sr}_2\text{Ca}_3\text{Cu}_4\text{O}_{12+y}$  superconductors, *J. Low Temp. Phys.* **156**, 22–29, (2009)
38. M. Tinkham, *Introduction to Superconductivity* (McGraw Hill, New York, 1996)
39. J.-J. Kim, H.-K. Lee, J. Chung, H.J. Shin, H.J. Lee, J.K. Ku, Flux-creep dissipation in epitaxial  $\text{YBa}_2\text{Cu}_3\text{O}_{7-\delta}$  film: Magnetic-field and electrical-current dependence. *Phys. Rev. B* **43**, 2962–2967 (1991)
40. M. Me. Barakat, K. Habanjar, Magneto-resistivity studies for BiPb-2223 phase added by BaSnO<sub>3</sub> nanoparticles, *J. Adv. Ceram.* **6**, 100–109, (2017)
41. M. Dogruer, Y. Zalaoglu, A. Varilci, C. Terzioglu, G. Yildirim, O. Ozturk, A study on magneto-resistivity, activation energy, irreversibility and upper critical field of slightly Mn added Bi-2223 superconductor ceramics. *J. Supercond. Nov. Magn.* **25**, 961–968 (2012)
42. N.R. Werthamer, E. Helfand, P.C. Hohenberg, Temperature and purity dependence of the superconducting critical field, Hc<sub>2</sub> III. Electron spin and spin-orbit effects, *Phys. Rev.*, **147**, 295–302, (1966)
43. Z.S., Wang, H.Q., Luo, C., Ren, H.H., Wen, Upper critical field, anisotropy, and superconducting properties of  $\text{Ba}_{1-x}\text{K}_x\text{Fe}_2\text{As}_2$  single crystals. *Phys. Rev., B* **78**, 140501 (R), (2008)
44. H.C. Yang, L.M. Wang, H.E. Horng, Characteristics of flux pinning in  $\text{YBa}_2\text{Cu}_3\text{O}_y/\text{PrBa}_2\text{Cu}_3\text{O}_y$  superlattices. *Phys. Rev. B* **59**, 8956–8961 (1999)
45. G. Yildirim, Formation of artificial flux pinning centers in Bi-2223 cuprate superconductor with Ni impurities and enhanced resistant to thermal fluxon motions of correlated 2D pancake vortices in new matrix. *J. Alloys Compd.* **745**, 100–110 (2018)
46. Y. Zalaoglu, G. Yildirim, H. Buyukuslu, N.K. Saritekin, A. Varilci, C. Terzioglu, O. Gorur, Important defeats on pinning of 2D pancake vortices in highly anisotropic Bi-2212 superconducting matrix with homovalent Bi/La substitution. *J. Alloys Compd.* **631**, 111–119 (2015)

**Publisher's Note** Springer Nature remains neutral with regard to jurisdictional claims in published maps and institutional affiliations.